Second-order parametric interactions in 1-D photonic-crystal microcavity structures

Mohammed F. Saleh, Luca Dal Negro and Bahaa E. A. Saleh

Department of Electrical and Computer Engineering, Boston University, Boston, MA 02215, USA

mohsaleh@bu.edu

Abstract: We develop a generalized model for studying second-order parametric interactions in 1-D multilayered photonic structures, accounting for collinear oblique waves and partial pump depletion. This model is used to assess the performance of parametric devices in photonic-crystal microcavity (PCM) structures. Our model shows dramatic enhancement of nonlinear interactions at frequencies for which the waves are localized. Also, we demonstrate the exponential dependence of the conversion efficiency of second harmonic generation (SHG) on the number of layers as was recently pointed out. In addition, in optical parametric amplification (OPA), we find that the gain has a resonance-like dependence on the pump intensity, turning large peak gain into strong attenuation at greater intensities, which suggests that the device can operate as an optical switch.

OCIS codes: (190.0190) Nonlinear optics; (130.3120) Integrated optics devices.

References and links

1. G. D'Aguanno, M. Centini, M. Scalora, C. Sibilia, M. Bertolotti, M. J. Bloemer, and C. M. Bowden, "Pulsed second-harmonic generation in nonlinear, one-dimensional, periodic structures," Phys. Rev. A **56**, 3166–3174 (1997).
2. M Soljacic and J. D. Joannopoulos, "Enhancement of nonlinear effects using photonic crystals," Nature (London) **3**, 211–219 (2004).
3. M. J. Steel and C. M. de Sterke, "Second-harmonic generation in second-harmonic fiber Bragg gratings," Appl. Opt. **35**, 3211–3222 (1996).
4. T. Ochiai and K. Sakoda, "Scaling law of enhanced second harmonic generation in finite Bragg stacks," Opt. Express **13**, 9094–9114 (2005).
5. J. W. Haus, R. Viswanathan, M. Scalora, A. G. Kalocsai, J. D. Cole, and J. Theimei, "Enhanced second-harmonic generation in media with a weak periodicity," Phys. Rev. A **57**, 2120–2128 (1998).
6. A. Arraf and C. M. de Sterke, "Coupled-mode equations for quadratically nonlinear deep gratings," Phys. Rev. E **58**, 7951–7958 (1998).
7. G. D'Aguanno, M. Centini, M. Scalora, C. Sibilia, M. Bertolotti, M. J. Bloemer, and C. M. Bowden, "Generalized coupled-mode theory for $\chi^{(2)}$ interactions in finite multilayered structures," J. Opt. Soc. Am. B **19**, 2111–2121 (2002).
8. A. N. Vamivakas, B. E. A. Saleh, A. V. Sergienko, and M. C. Teich, "Theory of spontaneous parametric down-conversion from photonic crystals," Phys. Rev. A **70**, 043810 (2004).
9. M. Centini, J. Peina, Jr., L. Sciscione, C. Sibilia, M. Scalora, M. J. Bloemer, and M. Bertolotti, "Entangled photon pair generation by spontaneous parametric down-conversion in finite-length one-dimensional photonic crystals," Phys. Rev. A **72**, 033806 (2005).
10. G. D'Aguanno, M. Centini, M. Scalora, C. Sibilia, Y. Dumeige, P. Vidakovic, J. A. Levenson, M. J. Bloemer, C. M. Bowden, J. W. Haus, and M. Bertolotti, "Photonic band edge effects in finite structures and applications to $\chi^{(2)}$ interactions," Phys. Rev. E **64**, 016609 (2001).

#92269 - $15.00 USD Received 30 Jan 2008; revised 18 Mar 2008; accepted 19 Mar 2008; published 1 Apr 2008

11. N. Mattiucci, G. D'Aguanno, M. Scalora, and M. J. Bloemer, "Coherence length for second-harmonic generation in nonlinear, one-dimensional, finite, multilayered structures," J. Opt. Soc. Am. B **24**, 877–886 (2007).
12. D. S. Bethune, "Optical harmonic generation and mixing in multilayer media: analysis using optical transfer matrix techniques," J. Opt. Soc. Am. B **6**, 910–916 (1989).
13. Y. Jeong and B. Lee, "Matrix analysis for layered quasi-phase-matched media considering multiple reflection and pump wave depletion," IEEE J. Quantum Electron. **35**, 162–172 (1999).
14. M. Cherchi, "Exact analytic expressions for electromagnetic propagation and optical nonlinear generation in finite one-dimensional periodic multilayers," Phys. Rev. E **69**, 066602 (2004).
15. L.-M Zhao, and B.-Y. Gu, "Giant enhancement of second harmonic generation in multiple photonic quantum well structures made of nonlinear material," Appl. Phys. Lett. **88**, 122904 (2006).
16. J. J. Li, Z. Y. Li, and D. Z. Zhang, "Second harmonic generation in one-dimensional nonlinear photonic crystals solved by the transfer matrix method," Phys. Rev. E **75**, 056606 (2007).
17. T. V. Dolgova, A. I. Maidykovski, M. G. Martemyanov, A. A. Fedyanin, O. A. Aktsipetrov, G. Marowsky, V. A. Yakovlev, and G. Mattei, "Giant microcavity enhancement of second-harmonic generation in all-silicon photonic crystals," Appl. Phys. Lett. **81**, 2725–2727 (2002).
18. M. Liscidinia and L. Andreani, "Highly efficient second-harmonic generation in doubly resonant planar microcavities," Appl. Phys. Lett. **85**, 1883–1885 (2004).
19. Y. Dumeige, I. Sagnes, P. Monnier, P. Vidakovic, I. Abram, C. Meriadec, and A. Levenson, "Phase-matched frequency doubling at photonic band edges: efficiency scaling as the fifth power of the length," Phys. Rev. Lett. **89**, 043901 (2002).
20. B. E. A. Saleh, M. C. Teich, *Fundamentals of Photonics* (Wiley, New York, 2007).
21. D. Y. K. Ko and J. R. Sambles, "Scattering matrix method for propagation of radiation in stratified media: attenuated total reflection studies of liquid crystals," J. Opt. Soc. Am. A **5**, 1863–1866 (1988).
22. M. Hiltunen, L. Dal Negro, N. -N. Feng, L. C. Kimerling, and J. Michel, "Modeling of aperiodic fractal waveguide structures for multifrequency light transport," J. Lightwave Technol. **25**, 1841–1847 (2007).
23. W. E. Angerer, N. Yang, A. G. Yodh, M. A. Khan, and C. J. Sun, "Ultrafast second-harmonic generation spectroscopy of GaN thin films on sapphire," Phys. Rev. B **59**, 2932–2946 (1999).
24. A. R. Cowan and J. F. Young, "Optical bistability involving photonic crystal microcavities and Fano line shapes," Phys. Rev. E **68**, 046606 (2003).
25. M. Ghulinyan C. J. Oton, G. Bonetti, Z. Gaburro, and L. Pavesi, "Free-standing porous silicon single and multiple optical cavities," J. Appl. Phys. **93**, 9724–9729 (2003).

1. Introduction

Multilayered structures and photonic crystals have attracted considerable attention in the last decade. These structures are characterized by localized states at which propagating waves are slowed down and hence nonlinear interactions are strengthened in comparison with bulk crystals of the same physical length [1]. Because of their miniaturized nature they are envisioned to enable low-power all-optical signal processing within integrated photonic chips [2].

The modeling of nonlinear parametric interactions in multilayered structures is difficult since it involves nonlinear three- or four-wave mixing in the presence of multiple reflections. A number of methods have been developed for one-dimensional structures, including the Green's function method [3-4], the multiple-scale method [5-9], the effective medium method [10-11], and the transfer matrix method [12-16]. Each of these methods is limited by certain requirements and assumptions such as the limitation to periodic structures, the use of the undepleted pump approximation, the requirement that the interacting waves propagate along the normal axis of the structure, and the limitation to a particular type of nonlinear interaction. One or more of these requirements may not be applicable in certain cases. For example, in the case of microcavity photonic structures, strong localized resonance states can lead to dramatic enhancement of the nonlinear interaction [17-18], and the use of the undepleted pump approximation may not be appropriate. Also, the group symmetry of some semiconductor materials, such as GaAs and related compounds, may inhibit second-order nonlinear processes at normal incidence [19], thereby necessitating operation at an oblique angle.

In this paper, we present a more general model based on a generalized matrix approach that circumvents the above limitations, and also avoids certain pitfalls [13] in earlier models based on matrix methods. Using our new formalism, we can describe second-order parametric non-

#92269 - $15.00 USD Received 30 Jan 2008; revised 18 Mar 2008; accepted 19 Mar 2008; published 1 Apr 2008

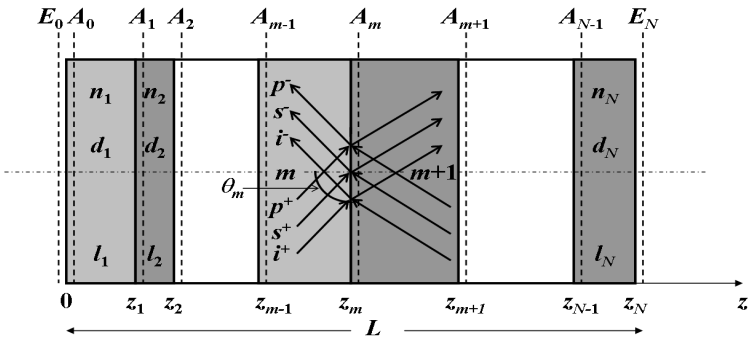

Fig. 1. An N-layer photonic structure. The mth layer has refractive index n_m, second-order nonlinear coefficient d_m and thickness l_m. The overall length is L. The forward waves are incident on the mth interface at an oblique angle θ_m. There are two sets of waves in the forward and backward directions: pump (p), signal (s) and idler (i). The superscripts $+$ and $-$ denote the forward and backward waves, respectively. The complex envelope at the left and right sides of the mth element are A_{m-1} and A_m, respectively. E_0 and E_N are the complex amplitudes at the left and right sides of the structure, respectively.

linear interactions of all types in a one-dimensional arbitrary multilayered structure (periodic, or non-periodic). The interacting waves are assumed to be collinear within any layer but may propagate at oblique directions with respect to the axis of the structure. Partial depletion of the pump is taken into account by use of an iterative method. We use the new formalism to analyze and design devices based on nonlinear parametric interactions in photonic-crystal structures with microcavities, and undertake a parametric study of the performance of these devices when used for second-harmonic generation (SHG), optical parametric amplification (OPA), and optical frequency conversion (OFC). Our goal is to highlight the dependence of the device performance on factors such as the frequencies of the three waves in relation to the frequencies of the localized states, the pump intensity, and the number of layers.

2. Matrix theory of nonlinear multilayered structures

In this section, we develop a model for three-wave mixing in a nonlinear 1-D structures composed of N layers. For simplicity, anistropic effects are not considered. As illustrated in Fig. 1, three waves, pump p^+, signal s^+, and idler i^+, are assumed to travel through the structure in the forward direction at an input angle θ_0 with the axis of the structure. Within each layer, these collinear co-directional waves are mutually coupled by the parametric interaction process. As a result of reflections at the layer boundaries, another set of collinear backward waves (p^-, s^-, and i^-) are generated at angles in each layer dictated by Snell's law. Each forward wave is coupled to a corresponding backward wave of the same frequency, and the backward waves are also mutually coupled within each layer via parametric interaction. We therefore have a total of six waves (p^+, p^-, s^+, s^-, i^+, i^-) interacting self-consistently within the structure in two ways: *i*) At each frequency, the forward and backward waves are pairwise coupled by multiple reflections at the boundaries (p^+ with p^-, s^+ with s^-, and i^+ with i^-). *ii*) In each direction, the forward waves (p^+, s^+, i^+) within each layer are coupled by the parametric process; the backward waves (p^-, s^-, i^-) are similarly coupled.

Linearization and matrix representation. Since the multi-reflection coupling between the forward and backward waves at each frequency is a linear effect, it can be readily modeled

#92269 - $15.00 USD Received 30 Jan 2008; revised 18 Mar 2008; accepted 19 Mar 2008; published 1 Apr 2008

by use of matrix methods. However, the parametric coupling between triplets of co-directional waves within a layer is nonlinear, and is therefore not amenable to matrix description. This problem is alleviated if the pump is assumed to be undepleted since the parametric relation between s^+ and i^+ (and also between s^- and i^-) will be linearized. For each layer, the reflection coupling is pairwise between each forward and backward wave of the same frequency, the parametric coupling is pairwise (signal to idler) for each direction, and the pump is constant. The relation between the six waves (p^+, p^-, s^+, s^-, i^+, i^-) at the input and output of a layer will then be described by a 6×6 matrix, denoted $\mathbf{T}_m$ for the mth layer. Under the undepleted pump approximation, the pump is assumed to be constant within each layer, albeit not the same in the different layers. The matrix $\mathbf{T}_m$ therefore has a block structure comprising a 2×2 matrix $\mathbf{T}_m^{(p)}$, which represents the independent transmission of the two pump waves (p^+, p^-) through the layer, and a 4×4 matrix $\mathbf{T}_m^{(s,i)}$, which represents the transmission of the four signal and idler waves (s^+, i^+, s^-, i^-) through the layer . We will refer to the matrices $\mathbf{T}_m^{(p)}$ and $\mathbf{T}_m^{(s,i)}$ as the pump block transfer matrix and the signal-idler block transfer matrix, respectively. A global matrix $\mathbf{T}$ for a structure made of N layers is the product of the layer matrices $\mathbf{T}_m$, where $m = 1, 2, \cdots, N$. Clearly, $\mathbf{T}$ will maintain the same block structure, and the matrix multiplication can be done separately for the 4×4 matrices $\mathbf{T}_m^{(s,i)}$ and the 2×2 matrices $\mathbf{T}_m^{(p)}$.

Envelope-amplitude correction. The use of matrix methods to describe light propagation in multilayered linear dielectric structures is well established in the literature [20]. The use of matrix methods to describe parametric wave mixing in homogeneous nonlinear media under the undepleted pump approximation is also straightforward. However, the use of matrix methods to describe propagation in nonlinear multilayered (piecewise homogenous) structures under the same approximations poses a subtle difficulty that has escaped some authors [13], leading to erroneous and inconsistent results. This difficulty has to do with the slowly varying envelope approximation usually used to write the parametric coupled equations in wave mixing. Since different layers of the structure have different refractive indexes, i.e., different propagation coefficients, we must switch back and forth between the complex amplitude (CA) and the complex envelope (CE) of the wave in order to use the appropriate "carrier" for each layer. This is afforded by defining an envelope-amplitude diagonal matrix $\mathbf{P}$ that converts the CE's into CA's whenever a new layer is entered. If $\mathbf{E}_m = [E_m^{(p^+)}\ E_m^{(p^-)}\ E_m^{(s^+)}\ E_m^{(s^-)}\ E_m^{(i^+)}\ E_m^{(i^-)}]^t$ and $\mathbf{A}_m = [a_m^{(p^+)}\ a_m^{(p^-)}\ a_m^{(s^+)}\ a_m^{(s^-)}\ a_m^{(i^+)}\ a_m^{(i^-)}]^t$ are vectors representing the CA's and CE's of the six waves at the right side of the mth element, respectively, then $\mathbf{E}_m = \mathbf{P}_m\mathbf{A}_m$. The superscript t refers to the matrix tranpose. In fact, disregarding the CA's to CE's conversion at the multilayered interfaces leads to unphysical solutions when the limiting case of a bulk homogeneous medium is considered. For instance, if a bulk homogeneous medium were reduced to N-layers, this method will lead to different answers for different values of N. Our model remedies this shortcoming.

Generalized transfer matrix. The 6×6 generalized transfer matrix that relates the CE's at the left and right sides of the mth layer can be written as a product of four matrices:

$$\mathbf{T}_m = \mathbf{P}_m^{-1}\mathbf{B}_m\mathbf{P}_m\mathbf{C}_m, \tag{1}$$

where $\mathbf{B}_m$ represents the boundary matrix and $\mathbf{C}_m$ represents the parametric-interaction matrix. The matrices $\mathbf{B}_m$, $\mathbf{P}_m$, and $\mathbf{C}_m$ have block structures and each one may be separated into a pump block and a signal-idler block, denoted ($\mathbf{B}_m^{(p)}$ and $\mathbf{B}_m^{(s,i)}$), ($\mathbf{P}_m^{(p)}$ and $\mathbf{P}_m^{(s,i)}$), and ($\mathbf{C}_m^{(p)}$ and $\mathbf{C}_m^{(s,i)}$). Each of these matrices is now considered in turn.

#92269 - $15.00 USD Received 30 Jan 2008; revised 18 Mar 2008; accepted 19 Mar 2008; published 1 Apr 2008

Boundary matrix. Using the Fresnel's refraction/reflection equations, the pump and the signal-idler boundary matrices of the mth element are [20]:

$$\mathbf{B}_m^{(p)} = \begin{bmatrix} B_m(p^+,p^+) & B_m(p^+,p^-) \\ B_m(p^-,p^+) & B_m(p^-,p^-) \end{bmatrix}, \mathbf{B}_m^{(s,i)} = \begin{bmatrix} B_m(s^+,s^+) & B_m(s^+,s^-) & 0 & 0 \\ B_m(s^-,s^+) & B_m(s^-,s^-) & 0 & 0 \\ 0 & 0 & B_m(i^+,i^+) & B_m(i^+,i^-) \\ 0 & 0 & B_m(i^-,i^+) & B_m(i^-,i^-) \end{bmatrix}, \tag{2}$$

where

$$B_m(q^\pm,q^\pm) = \begin{cases} \left(n_m^{(q)}\cos\theta_m^{(q)} + n_{m-1}^{(q)}\cos\theta_{m-1}^{(q)}\right)/2n_m^{(q)}\cos\theta_m^{(q)} & \text{TE}-\text{polarization} \\ \left(n_m^{(q)}\sec\theta_m^{(q)} + n_{m-1}^{(q)}\sec\theta_{m-1}^{(q)}\right)\cos\theta_{m-1}^{(q)}/2n_m^{(q)} & \text{TM}-\text{polarization} \end{cases},$$

$$B_m(q^\pm,q^\mp) = \begin{cases} \left(n_m^{(q)}\cos\theta_m^{(q)} - n_{m-1}^{(q)}\cos\theta_{m-1}^{(q)}\right)/2n_m^{(q)}\cos\theta_m^{(q)} & \text{TE}-\text{polarization} \\ \left(n_m^{(q)}\sec\theta_m^{(q)} - n_{m-1}^{(q)}\sec\theta_{m-1}^{(q)}\right)\cos\theta_{m-1}^{(q)}/2n_m^{(q)} & \text{TM}-\text{polarization} \end{cases}, \tag{3}$$

$$n_m^{(q)}\sin\theta_m^{(q)} = n_{m-1}^{(q)}\sin\theta_{m-1}^{(q)} = n_0^{(q)}\sin\theta_0^{(q)}, \qquad q = p,s,i,$$

and $n_k^{(q)}$ and $\theta_k^{(q)}$ are the refractive index and the angle of the wave q in the kth layer. The subscript 0 is associated with the embedding medium. Since $\theta_k^{(q)}$ is almost unaltered for the three interacting waves, it is assumed to be approximately frequency independent and is denoted θ_k.

Envelope-amplitude matrix. This is a diagonal matrix whose elements represent the phase accumulated by each wave from the beginning of the structure until the end of the current element,

$$\mathbf{P}_m^{(p)} = \begin{bmatrix} \Phi_m^{(p^+)} & \Phi_m^{(p^-)} \end{bmatrix} \mathbf{I}_{2\times2}, \quad \mathbf{P}_m^{(s,i)} = \begin{bmatrix} \Phi_m^{(s^+)} & \Phi_m^{(s^-)} & \Phi_m^{(i^+)} & \Phi_m^{(i^-)} \end{bmatrix} \mathbf{I}_{4\times4}, \tag{4}$$

where

$$\Phi_m^{(q^\pm)} = \exp\left(\mp j\frac{1}{c}\sum_{k=1}^{k=m} n_k^{(q)}\,\omega_q\,l_k\cos\theta_k\right), \qquad q = p,s,i, \tag{5}$$

$\mathbf{I}$ is the unity matrix, l_k is the length of the kth element, ω_q is the angular frequency of the wave q, and c is the velocity of light in free space. This formula accounts for the insertion of the operator $\mathbf{P}_m^{-1}$ in Eq. (1).

Parametric-interaction matrix. At normal incidence, the nonlinear interactions between the waves in each of the forward and backward directions are governed by the coupled-mode equations, which are based on the slowly varying envelope approximation. Within the mth layer which is located in the interval $z_{m-1} \leqslant z \leqslant z_m$, these equations are [20]:

$$\begin{aligned} \frac{da_m^{(u^\pm)}}{dz} &= \mp j g_m^{(u)}\, a_m^{(w^\pm)} a_m^{(v^\pm)*} \exp(\mp j\Delta k_m z), \\ \frac{da_m^{(v^\pm)}}{dz} &= \mp j g_m^{(v)}\, a_m^{(w^\pm)} a_m^{(u^\pm)*} \exp(\mp j\Delta k_m z), \\ \frac{da_m^{(w^\pm)}}{dz} &= \mp j g_m^{(w)}\, a_m^{(u^\pm)} a_m^{(v^\pm)} \exp(\pm j\Delta k_m z), \end{aligned} \tag{6}$$

#92269 - $15.00 USD Received 30 Jan 2008; revised 18 Mar 2008; accepted 19 Mar 2008; published 1 Apr 2008

where

$$\Delta k_m = \frac{1}{c}\left(n_m^{(w)}\omega_w - n_m^{(u)}\omega_u - n_m^{(v)}\omega_v\right), \qquad g_m^{(q)} = 120\pi\, d_m \omega_q / n_m^{(q)}, \qquad u,v,w,q = p,s,i, \quad (7)$$

d_m is the second-order nonlinear coefficient of the mth element, and the superscript * represents the complex conjugate. Under the undepleted pump approximation, the pump differential equation is ignored and the other two equations can be solved and cast in a matrix form,

$$\mathbf{C}_m^{(p)} = \begin{bmatrix} 1 & 0 \\ 0 & 1 \end{bmatrix}, \qquad \mathbf{C}_m^{(s,i)} = \begin{bmatrix} C_{m\,(s^+,s^+)} & 0 & C_{m\,(s^+,i^+)} & 0 \\ 0 & C_{m\,(s^-,s^-)} & 0 & C_{m\,(s^-,i^-)} \\ C_{m\,(i^+,s^+)} & 0 & C_{m\,(i^+,i^+)} & 0 \\ 0 & C_{m\,(i^-,s^-)} & 0 & C_{m\,(i^-,i^-)} \end{bmatrix}, \quad (8)$$

where the elements of the $\mathbf{C}_m^{(s,i)}$ matrix depend on the average value of the CE of the pump wave within the mth layer as well as the type of parametric application, as will be shown in the next section. For oblique waves propagating at an angle θ_m, the solution of Eq. (6) is applicable if l_m is replaced by $l_m/\cos\theta_m$ since the waves then propagate a longer distance within the layer. Another deficiency in the model described in [13] is that the derivation of these matrix elements is based on a value $z_{m-1} = 0$ for all the layers, which is incorrect except for the first layer.

Transmission through cascaded elements. The CE's at the right side of the mth element are given by:

$$\mathbf{A}_m^{(q)} = \mathbf{T}_m^{(q)}\mathbf{T}_{m-1}^{(q)} \cdots \mathbf{T}_2^{(q)}\mathbf{T}_1^{(q)}\mathbf{B}_0^{(q)}\mathbf{E}_0^{(q)}, \qquad \begin{cases} q = p \\ q = s,i \end{cases}, \quad (9)$$

where

$$\begin{aligned} \mathbf{E}_0^{(p)} &= \begin{bmatrix} E_0^{(p^+)} & E_0^{(p^-)} \end{bmatrix}^t, \quad \mathbf{E}_0^{(s,i)} = \begin{bmatrix} E_0^{(s^+)} & E_0^{(s^-)} & E_0^{(i^+)} & E_0^{(i^-)} \end{bmatrix}^t, \\ \mathbf{A}_m^{(p)} &= \begin{bmatrix} a_m^{(p^+)} & a_m^{(p^-)} \end{bmatrix}^t, \quad \mathbf{A}_m^{(s,i)} = \begin{bmatrix} a_m^{(s^+)} & a_m^{(s^-)} & a_m^{(i^+)} & a_m^{(i^-)} \end{bmatrix}^t. \end{aligned} \quad (10)$$

Since the CE is the same as the CA at $z = 0$, there is no need to use $\left[\mathbf{P}_0^{(q)}\right]^{-1}$ at this boundary.

Pump depletion. To take into account the depletion of the pump, an iterative technique based on perturbation theory is used such that at any step of the iteration, the coupling between each co-directional signal-idler pair is linearized. The solution under the undepleted pump approximation is used as the first iteration. The spatial distributions of the signal and the idler are then computed within each layer. Given these distributions, the parametric equations describing the evolution of the pumps within the layer are resolved to determine updated distributions, which will no longer be constant within each layer. Using the values of the CE's at the beginning and at the end of each layer, average values of the CE's are then determined for the forward and the backward pumps. These values are used as fixed values to determine elements of a revised signal-idler 4×4 submatrix $\mathbf{T}_m^{(s,i)}$, which is used again to obtain better average values of the pumps within each layer. The process may be repeated until convergence is reached, but since convergence is not assured, this perturbation theory technique may not be applicable in cases of very strong pump depletion.

Based on this perturbation approach, Eq. (9) is modified to

$$\mathbf{A}_m^{(p)} = \mathbf{T}_m^{(p)}\mathbf{T}_{m-1}^{(p)} \cdots \mathbf{T}_2^{(p)}\mathbf{T}_1^{(p)}\mathbf{B}_0^{(p)}\mathbf{E}_0^{(p)} + \mathbf{X}_m^{(p)}, \quad (11)$$

#92269 - $15.00 USD Received 30 Jan 2008; revised 18 Mar 2008; accepted 19 Mar 2008; published 1 Apr 2008

where

$$\mathbf{X}_m^{(p)} = \sum_{k=1}^{m} \mathbf{T}_m^{(p)} \mathbf{T}_{m-1}^{(p)} \cdots \mathbf{T}_k^{(p)} \begin{bmatrix} x_k^{(p^+)} \\ x_k^{(p^-)} \end{bmatrix} \tag{12}$$

and $x_k^{(p^+)}$ and $x_k^{(p^-)}$ are obtained from the perturbed pump differential equations in the kth layer. The first term in Eq. (11) is the outcome of the linear propagation in a multilayered structure, while the second results from the parametric interaction process.

Degenerate case. The above equations are the generalized equations applicable to all second-order parametric interactions in multilayered strutures. They can be readily specified to OPA or OFC. In the degenerate SHG case, the dimensionality of the signal-idler matrix is reduced to 2×2 and an equation similar to Eq. (11) (with p replaced by s) can be used instead of Eq. (9) to determine $\mathbf{A}_m^{(s)}$.

Transfer matrix vs scattering matrix. There are two approaches for relating the CE's at the sides of each layer: the transfer matrix **T** method and the scattering matrix **S** method [20]. The **T** matrix relates the CE's at right side to those at the left side, while the **S** matrix relates the incoming CE's from both sides to the outgoing CE's. The advantage of the transfer matrix method is that the total transfer matrix of the structure is the product of the transfer matrices of each layer in a reverse order. The advantage of the scattering matrix is that it is easier to write and interpret in terms of physical parameters. Commonly, the total transfer matrix of the entire structure is calculated first using transfer matrix multiplication, then it is converted into the scattering matrix to assess the performance of the structure. Since photonic structures can be characterized by strong forbidden bands within which a wave is completely reflected, the structure can act as a perfect mirror isolating the left and right sides of the structure. In this case, the transfer matrix method is not appropriate. Fortunately, this problem can be addressed by use of a new technique described in [21] for the 2×2 case, and can be generalized to describe the 6×6 scattering matrix **S** of our multilayered structure for the entire band of frequencies of interest. This **S** matrix will preserve the block structure, i.e., has a pump block $\mathbf{S}^{(p)}$ and a signal-idler block $\mathbf{S}^{(s,i)}$.

Summary of the computational procedure. The computational procedure is based on an iterated two-step process for which the pump dynamics are considered with given signal and idler distributions and then the signal-idler dynamics are considered with fixed pump:

1. Determine the distributions of the forward and backward pumps in the absence of parametric interaction. Using the matrices $\mathbf{T}_m^{(p)}$ for all the layers, the overall pump scattering matrix $\mathbf{S}^{(p)}$ is determined. Knowing the input pump waves, $\mathbf{A}_m^{(p)}$ is calculated for $m = 0, \cdots, N$.

2. Taking the pump distributions in step 1 to be fixed (undepleted), determine the signal-idler matrix $\mathbf{T}_m^{(s,i)}$ for all the layers and calculate the overall signal-idler scattering matrix $\mathbf{S}^{(s,i)}$. Knowing the input signal and idler waves, the output waves can be calculated.

   The results of steps 1 and 2 represent the solution of the three-wave mixing problem under the undepleted pump approximation.

3. Using the signal-idler values $\mathbf{E}_0^{(s,i)}$ and $\mathbf{T}_m^{(s,i)}$, determine $\mathbf{A}_m^{(s,i)}$ and use it to compute $\mathbf{X}_N^{(p)}$ and *new* values for the output pump fields $E_N^{(p^+)}$ and $E_0^{(p^-)}$.

#92269 - $15.00 USD Received 30 Jan 2008; revised 18 Mar 2008; accepted 19 Mar 2008; published 1 Apr 2008

4. Using $\mathbf{E}_0^{(p)}$, $\mathbf{T}_m^{(p)}$, and $\mathbf{X}_m^{(p)}$, determine $\mathbf{A}_m^{(p)}$, which may be used to compute the *new* $\mathbf{T}_m^{(s,i)}$ and the *new* output signal and idler waves.

5. Repeat steps 3 and 4 and monitor the normalized error in the conservation of energy,

$$\Delta = \left| \frac{I_{output} - I_{input}}{I_{input}} \right|, \tag{13}$$

where I_{input} and I_{output} are the input and output intensities of the six interacting waves, respectively. The iterative process is terminated when Δ reaches 10^{-5}. If this value is not reached after 50 iterations, the results of the iteration with the minimum Δ are selected and reported, along with the associated error.

3. Parametric nonlinear interactions in quarter-wave stack microcavities

In this section, we use our model to study parametric nonlinear interactions in photonic-crystal microcavity (PCM) structures, which are characterized by strongly localized midgap resonance states at which the group velocity is strongly reduced, resulting in dramatic enhancement of the nonlinear interaction. We consider three applications: second-harmonic generation (SHG), optical parametric amplification (OPA), and optical frequency conversion (OFC).

In all applications, we assume a PCM structure embedded in air, as shown in Fig. 2(a). The crystal is made up of two alternating layers of GaN and air. The fabrication of the structure is compatible with standard deposition methods such as sputtering, chemical vapor deposition, etc. In addition, it has been recently proposed that similar structures can be conveniently integrated in waveguide geometry by consecutive deposition and etching steps [22]. Since GaN has a wide electronic bandgap, absorption can be neglected at wavelengths extending from the infrared to the visible regions. The material dispersion properties of GaN are described in [23] and the second-order nonlinear coefficient is assumed to be 10^{-22} F/V [9]; higher order nonlinear coefficients have been neglected as in [4]. However, these nonlinear effects can be important since, for instance, third-order nonlinearity in PCM structures with high index contrast and large number of layers may lead to important effects such as optical bistability [24]. On the other hand, the unavoidable optical losses associated with the fabrication of real 1-D structure [25] will reduce significantly the resonant character of the localized modes and therefore would prevent the onset of optical bistability. The waves are incident at $\theta_0 = 20^\circ$ on the left side of the structure and are TM polarized. The multilayered structure is made up of a quarter-wave stack, i.e., for each layer the optical path along the z-axis is equal to a quarter of a reference wavelength λ_B, corresponding to the midgap frequency ω_B (Bragg frequency),

$$n_1(\omega_B) l_1 \cos\theta_1 = n_2(\omega_B) l_2 \cos\theta_2 = \frac{\lambda_B}{4} = \frac{\pi c}{2\omega_B}, \tag{14}$$

where λ_B is chosen to be 1.5 μm.

3.1. *Second harmonic generation*

SHG is the degenerate case of three-wave mixing for which two waves, u and v, at the same frequency combine to generate a wave w at twice the frequency, i.e., $\omega_u = \omega_v$ and $\omega_w = 2\omega_u$. In this case, $u = v = p$ and $w = s$ so that the coupled mode equations in the kth layer are modified to:

$$\frac{da_k^{(p^\pm)}}{dz} = \mp j g_k^{(p)} a_k^{(s^\pm)} a_k^{(p^\pm)^*} \exp(\mp j \Delta k_k z), \tag{15}$$

$$\frac{da_k^{(s^\pm)}}{dz} = \mp j \frac{1}{2} g_k^{(s)} \left(a_k^{(p^\pm)} \right)^2 \exp(\pm j \Delta k_k z), \tag{16}$$

#92269 - $15.00 USD Received 30 Jan 2008; revised 18 Mar 2008; accepted 19 Mar 2008; published 1 Apr 2008

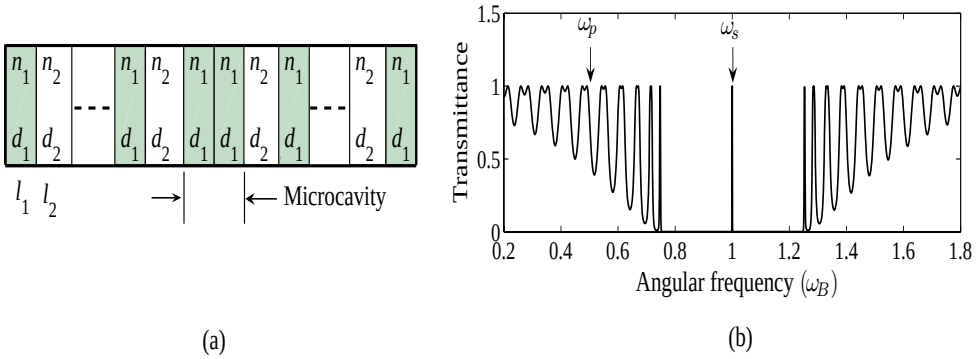

Fig. 2. (a) A 1-D photonic-crystal microcavity structure made up of two alternating layers: a GaN layer with thickness l_1, refractive index n_1 and nonlinear coefficient $d_1 = 10^{-22}\,F/V$; and an air layer with thickness l_2, $n_2 = 1$ and $d_2 = 0$. The crystal is made up of a quarter wave stack, with $1.5\,\mu$m as the reference wavelength. (b) Spectral characteristics of linear transmission through 50-layers structure (ω_B is the Bragg frequency).

where the factor $\frac{1}{2}$ is due to the degeneracy of the pump wave. The solution of Eq. (16) under the undepleted pump approximation is

$$a_k^{(s^\pm)}(z_k) = a_k^{(s^\pm)}(z_{k-1}) + x_k^{(s^\pm)}, \tag{17}$$

where

$$x_k^{(s^\pm)} = \mp j\,\alpha_k^{(s^\pm)} \mathrm{sinc}\left(\Delta k_k\, l_k/2\right) \exp\left[\pm j\Delta k_k\left(l_k + 2z_{k-1}\right)/2\right], \quad \alpha_k^{(s^\pm)} = \frac{1}{2} g_k^{(s)}\, l_k \left(\overline{a}_k^{(p^\pm)}\right)^2, \tag{18}$$

$\overline{a}_k^{(p^+)}$ and $\overline{a}_k^{(p^-)}$ are the average values of the CE of the forward and backward pump in the kth layer, respectively, and $\mathrm{sinc}(x) = \sin(x)/x$. The spatial dependence of the forward and backward pump waves can be obtained using the first-order perturbation theory,

$$a_k^{(p^\pm)}(z_k) = a_k^{(p^\pm)}(z_{k-1}) + x_k^{(p^\pm)}, \tag{19}$$

where

$$\begin{aligned} x_k^{(p^\pm)} &= \mp j\left[\alpha_k^{(p^\pm)} \mathrm{sinc}\left(\Delta k_k\, l_k/2\right) \exp\left(\mp j\Delta k_k\left(l_k + 2z_{k-1}\right)/2\right) + \beta_k^{(p^\pm)}\right], \\ \alpha_k^{(p^\pm)} &= g_k^{(p)}\, \overline{a}_k^{(p^\pm)^*}\left[l_k\, a_k^{(s^\pm)}(z_{k-1}) + \alpha_k^{(s^\pm)}/\Delta k_k \exp\left(\pm j\Delta k_k\, z_{k-1}\right)\right], \\ \beta_k^{(p^\pm)} &= -g_k^{(p)}\, \overline{a}_k^{(p^\pm)^*}\, \alpha_k^{(s^\pm)}/\Delta k_k. \end{aligned} \tag{20}$$

Using the analytical formulas of $x_k^{(s^\pm)}$ and $x_k^{(p^\pm)}$, we can determine the perturbed nonlinear second term in Eq. (11) for both the signal and the pump.

The performance of the SHG is determined by the forward and backward conversion efficiencies,

$$\eta^+ = \frac{I_N^{(s^+)}}{I_0^{(p^+)}}, \qquad \eta^- = \frac{I_0^{(s^-)}}{I_0^{(p^+)}}, \tag{21}$$

where $I_N^{(s^+)}$ and $I_0^{(s^-)}$ are the output intensities of the forward and backward signal waves, respectively, and $I_0^{(p^+)}$ is the input pump intensity.

#92269 - $15.00 USD Received 30 Jan 2008; revised 18 Mar 2008; accepted 19 Mar 2008; published 1 Apr 2008

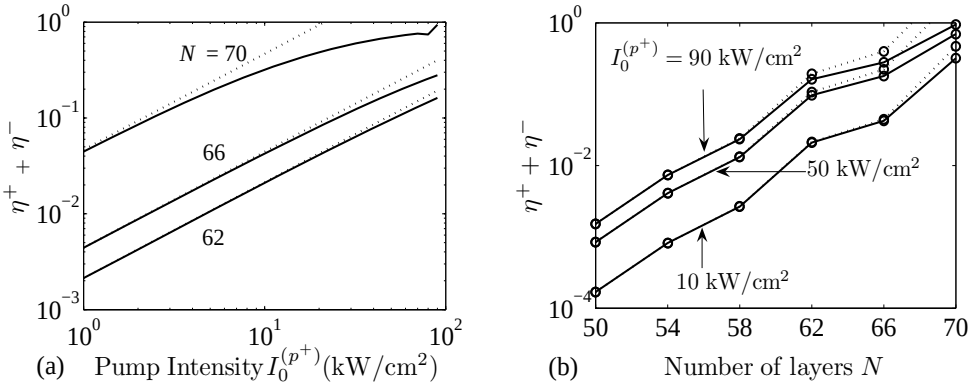

Fig. 3. Dependence of the total SHG conversion efficiency $\eta^+ + \eta^-$ on: (a) the pump intensity $I_0^{(p^+)}$, and (b) the number of layers *N*. The straight (dotted) lines represent values computed under the iterative perturbative technique (undepleted pump approximation).

When a pump wave at frequency $0.5\omega_B$ is incident on the PCM structure with the aforementioned characteristics, a second-harmonic wave at frequency ω_B is generated, as shown in Fig. 2(b), so that the signal is strongly localized within the structure. The localization of one of the interacting waves or both (if this is possible) turns out to produce a substantial enhancement of the nonlinear interaction (exceeding the enhancement attained by satisfying the phase matching condition in a homogeneous medium). Our calculations show that the use of the microcavity 1-D structure provides enhancement as high as 9 orders of magnitude, in comparison with a bulk homogeneous crystal of the same physical length. Additionally, the following important conclusions can be made:

- The dependence of the efficiency of SHG (in the forward and backward directions) on the pump intensity $I_0^{(p^+)}$ and the number of layers *N* in the limit of negligible pump depletion can be modeled by the expression,

$$\eta^+ + \eta^- \approx \zeta\, I_0^{(p^+)} \exp(N\varphi), \tag{22}$$

  where ζ and φ are constants that depend on the nonlinear coefficients, the dimensions and the refractive indexes of the alternating layers. This model is consistent with the results shown in Figs. 3(a) and 3(b), as will be elucidated in the following points.

- As shown in Fig. 3(a), in the undepleted pump regime, the efficiency of SHG increases linearly with increase of the pump intensity $I_0^{(p^+)}$. In a log-log scale, the slopes of the undepleted pump curves are approximately unity and do not depend on the number of periods. These curves are identical but shifted for different *N*. Saturation effects starts earlier as the number of layers increases, since the nonlinear interaction is strengthened as the interacting waves are slowed down. On $N = 70$, the kink occurring at $I_0^{(p^+)} \approx 80$ kW/cm^2, reflects the onset of strong pump depletion beyond the first-order approximation used in our perturbative approach. Therefore, for pump power larger than this threshold value, high-order perturbations would be required to ensure an improved level of accuracy.

- As shown in Fig. 3(b), the efficiency of SHG is approximately an exponential function of the number of layers *N* (with a fixed layer width), so that the dependence on the overall

#92269 - $15.00 USD Received 30 Jan 2008; revised 18 Mar 2008; accepted 19 Mar 2008; published 1 Apr 2008

device length is approximately exponential. This result agrees with previous results [4] and [18]. The slight variation around the linear model, which appears in a semilog scale, arises from altering the linear and the nonlinear interactions among the waves as the number of layers varies by discrete values. The mathematical model in Eq. (22) does not describe the small variations.

- As either $I_0^{(p^+)}$ or N increases, the undepleted pump approximation fails and significant violation of conservation of energy is observed. However, our iterative perturbative technique brings this error down (e.g., the maximum error of Δ in all the cases that we computed is reduced from 4.2 to 4×10^{-2}).

3.2. *Optical parametric amplification*

In OPA, a signal wave u is amplified in the presence of a pump wave w; an idler wave v is generated in the process. Here, $u=s$, $v=i$, $w=p$, and $\omega_s+\omega_i=\omega_p$. Solving the coupled mode equations under the undepleted pump approximation, the elements of the signal-idler parametric-interaction matrix of the kth layer are given by

$$\begin{aligned}
C_{k\,(s^\pm,s^\pm)} &= \exp\left(\mp\sigma_k l_k\right)\left[\cosh\left(\gamma_k^\pm l_k\right)\pm\frac{\sigma_k}{\gamma_k^\pm}\sinh\left(\gamma_k^\pm l_k\right)\right],\\
C_{k\,(s^\pm,i^\pm)} &= \mp j\frac{g_k^{(s)}\,\overline{a}_k^{(p^\pm)}}{\gamma_k^\pm}\exp\left[\mp\sigma_k\left(l_k+2z_{k-1}\right)\right]\sinh\left(\gamma_k^\pm l_k\right),\\
C_{k\,(i^\pm,s^\pm)} &= \pm j\frac{g_k^{(i)}\,\overline{a}_k^{(p^\pm)\,*}}{\gamma_k^\pm}\exp\left[\pm\sigma_k\left(l_k+2z_{k-1}\right)\right]\sinh\left(\gamma_k^\pm l_k\right),\\
C_{k\,(i^\pm,i^\pm)} &= \exp\left(\pm\sigma_k l_k\right)\left[\cosh\left(\gamma_k^\pm l_k\right)\mp\frac{\sigma_k}{\gamma_k^\pm}\sinh\left(\gamma_k^\pm l_k\right)\right],\\
\gamma_k^\pm &= \left(\sigma_k^2+g_k^{(s)}\,g_k^{(i)}\left|\overline{a}_k^{p^\pm}\right|^2\right)^{1/2},\qquad \sigma_k = j\Delta k_k/2.
\end{aligned}\tag{23}$$

The matrix $\mathbf{C}_k^{(s,i)}$ relates the CE's of the signal and the idler *complex conjugate*. Consequently, the signal-idler envelope-amplitude matrix of the kth layer is modified to

$$\mathbf{P}_k^{(s,i)} = \left[\begin{array}{cccc}\Phi_k^{(s^+)} & \Phi_k^{(s^-)} & \Phi_k^{(i^+)^*} & \Phi_k^{(i^-)^*}\end{array}\right]\mathbf{I}_{4\times4}.\tag{24}$$

Using the first-order perturbation theory, the spatial dependence of the forward and backward pump waves are:

$$a_k^{(p^\pm)}(z_k) = a_k^{(p^\pm)}(z_{k-1}) + x_k^{(p^\pm)},\tag{25}$$

where

$$x_k^{(p^\pm)} = \begin{cases}
\dfrac{\mp j g_k^{(p)}}{2}\left[\alpha_k^\pm\dfrac{\cosh\left(\gamma_k^\pm l_k+\gamma_k^{\pm^*}l_k\right)-1}{\gamma_k^\pm+\gamma_k^{\pm^*}}+\beta_k^\pm\dfrac{\cosh\left(\gamma_k^\pm l_k-\gamma_k^{\pm^*}l_k\right)-1}{\gamma_k^\pm-\gamma_k^{\pm^*}}\right.\\
\qquad\left.+\xi_k^\pm\dfrac{\sinh\left(\gamma_k^\pm l_k+\gamma_k^{\pm^*}l_k\right)}{\gamma_k^\pm+\gamma_k^{\pm^*}}+\delta_k^\pm\dfrac{\sinh\left(\gamma_k^\pm l_k-\gamma_k^{\pm^*}l_k\right)}{\gamma_k^\pm-\gamma_k^{\pm^*}}\right], & \text{if } \gamma_k^\pm\neq\gamma_k^{\pm^*},\\
\dfrac{\mp j g_k^{(p)}}{2}\left[\alpha_k^\pm\dfrac{\cosh\left(2\gamma_k^\pm l_k\right)-1}{2\gamma_k^\pm}+\xi_k^\pm\dfrac{\sinh\left(2\gamma_k^\pm l_k\right)}{2\gamma_k^\pm}+\delta_k^\pm l_k\right], & \text{otherwise,}
\end{cases}$$

#92269 - $15.00 USD Received 30 Jan 2008; revised 18 Mar 2008; accepted 19 Mar 2008; published 1 Apr 2008

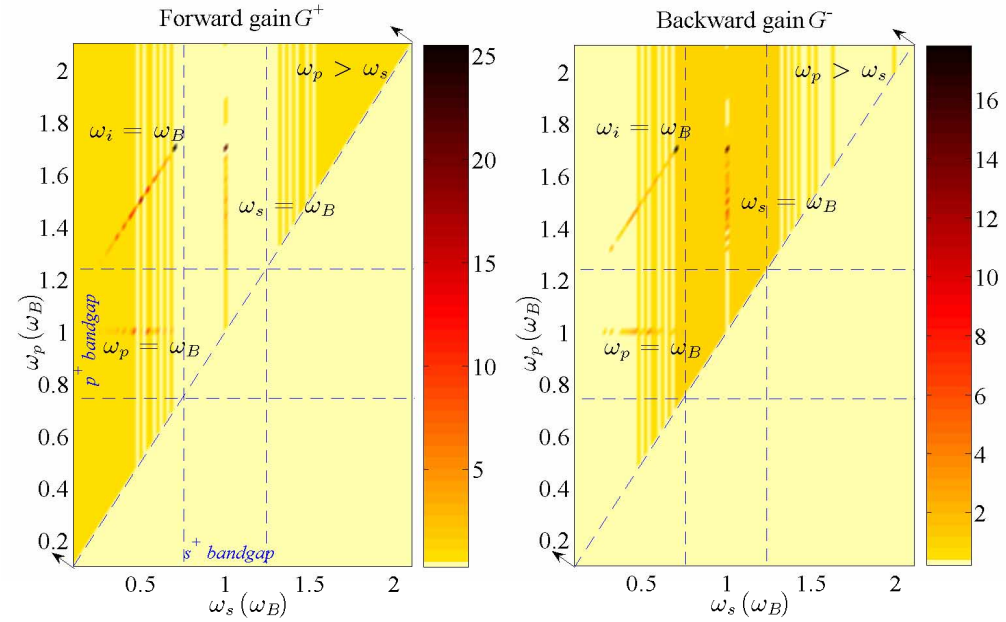

Fig. 4. (Color online). Dependence of the forward and backward gain on the signal and pump frequencies in units of ω_B.The dashed lines represent frequencies- and band-boundaries. The bright spots represent values of gain. The pump and signal intensities are 50 kW/cm^2 and 0.1 kW/cm^2, respectively, and the number of layers is 70. The forward and backward gain are enhanced at $\omega_p = \omega_B$, $\omega_s = \omega_B$ and $\omega_i = \omega_B$.

$$
\begin{aligned}
\alpha_k^{\pm} &= \mp j\left(\frac{g_k^{(i)}\,\overline{a}_k^{(p^\pm)^*}}{\gamma_k^{\pm^*}}\left|a_k^{(s^\pm)}\right|^2 + \frac{g_k^{(s)}\,\overline{a}_k^{(p^\pm)}}{\gamma_k^{\pm}}\left|a_k^{(i^\pm)}\right|^2\right) \pm \rho_k^{\pm} a_k^{(s^\pm)}\,a_k^{(i^\pm)}\left(\frac{\sigma_k}{\gamma_k^{\pm}} - \frac{\sigma_k^*}{\gamma_k^{\pm^*}}\right),\\
\beta_k^{\pm} &= \pm j\left(\frac{g_k^{(i)}\,\overline{a}_k^{(p^\pm)^*}}{\gamma_k^{\pm^*}}\left|a_k^{(s^\pm)}\right|^2 - \frac{g_k^{(s)}\,\overline{a}_k^{(p^\pm)}}{\gamma_k^{\pm}}\left|a_k^{(i^\pm)}\right|^2\right) \pm \rho_k^{\pm} a_k^{(s^\pm)}\,a_k^{(i^\pm)}\left(\frac{\sigma_k}{\gamma_k^{\pm}} + \frac{\sigma_k^*}{\gamma_k^{\pm^*}}\right),\\
\xi_k^{\pm} &= \frac{1}{\left|\gamma_k^{\pm}\right|^2}\left[\rho_k^{\pm} a_k^{(s^\pm)}\,a_k^{(i^\pm)}\left(\left|\gamma_k^{\pm}\right|^2 - |\sigma_k|^2\right) - \rho_k^{\pm^*} g_k^{(s)} g_k^{(i)}\,a_k^{(s^\pm)^*} a_k^{(i^\pm)^*}\left|\overline{a}_k^{(p^\pm)}\right|^2\right.\\
&\qquad \left. - j g_k^{(i)}\,\sigma_k\,\overline{a}_k^{(p^\pm)^*}\left|a_k^{(s^\pm)}\right|^2 + j g_k^{(s)}\,\sigma_k^*\,\overline{a}_k^{(p^\pm)}\left|a_k^{(i^\pm)}\right|^2\right],\\
\delta_k^{\pm} &= \rho_k^{\pm} a_k^{(s^\pm)}\,a_k^{(i^\pm)} - \xi_k^{\pm}, \qquad \rho_k^{\pm} = \exp\left(\pm j\Delta k_k\, z_{k-1}\right),
\end{aligned}
\tag{26}
$$

and $a_k^{(s^\pm)} = a_k^{(s^\pm)}(z_{k-1})$ and $a_k^{(i^\pm)} = a_k^{(i^\pm)}(z_{k-1})$. The performance of OPA in a multilayered structure can be determined by the forward and backward gain,

$$
G^+ = \frac{I_N^{(s^+)}}{I_0^{(s^+)}}, \qquad G^- = \frac{I_0^{(s^-)}}{I_0^{(s^+)}}, \tag{27}
$$

where $I_0^{(s^+)}$ is the input signal intensity.

A pump wave with $I_0^{(p^+)}$ = 50 kW/cm^2 and a signal wave with $I_0^{(s^+)}$ = 0.1 kW/cm^2 are incident on a microcavity structure with $N = 70$. The dependence of the forward and backward gain on

#92269 - $15.00 USD Received 30 Jan 2008; revised 18 Mar 2008; accepted 19 Mar 2008; published 1 Apr 2008

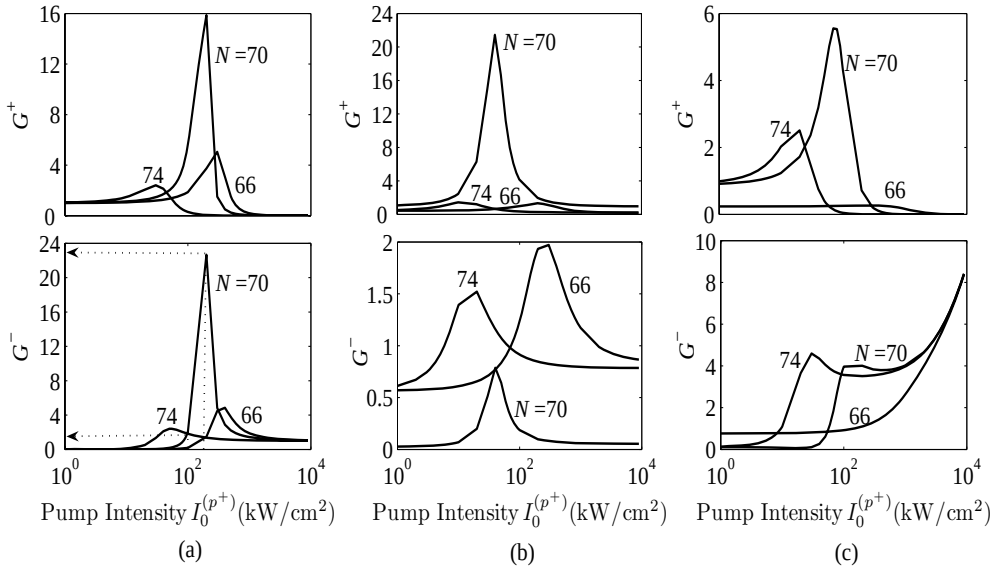

Fig. 5. Dependence of the forward and backward gain on the pump intensity $I_0^{(p^+)}$ for three values of the number of layers N. (a) $\omega_s = \omega_B$, $\omega_p = 1.3\omega_B$. (b) $\omega_s = 0.5\omega_B$, $\omega_p = 1.5\omega_B$. (c) $\omega_s = 0.6\omega_B$, $\omega_p = \omega_B$.

the signal and pump frequencies are plotted in Fig. 4. Since in this process, $\omega_p = \omega_s + \omega_i$, so that we are limited to the domain $\omega_p > \omega_s$. For a quarter-wave stack, the spectral dependence is periodic with a period $2\omega_B$. Nonlinear effects are strong only if one of the interacting waves is at the resonant midgap frequency, i.e., $\omega_p = \omega_B$, $\omega_s = \omega_B$ and $\omega_i = \omega_B$. At each of these three lines, localization within the structure plays a dominant role in the gain enhancement, while factors such as the phase mismatching and the frequency dependence of the coefficients $g_k^{(q)}$, $q = p, s, i$ are less significant. Of course, the gain enhancement along the three localization lines ceases if the frequency of one of the interacting waves lies in the forbidden band. Although, the incident waves are in the forward direction, there is an enhancement in the backward gain along these three lines. This is because the strong localized wave suffers multiple reflections that has the same effect as an incident wave on the right side of the structure. Elsewhere in the diagram, the signal wave propagates linearly, for instance, a signal wave that has frequency within the bandgap suffers complete reflection. The iterative perturbative technique reduces the maximum error in Δ from 0.21 to 0.02.

The dependence of the forward and backward gain on the pump intensity $I_0^{(p^+)}$ is plotted in Fig. 5 with the number of layers N as a parameter. Three points on the localized-state frequency lines, one on each line, are used for these plots. The dependence of the gain on the pump intensity exhibits a resonance-like behavior when either $\omega_s = \omega_B$ or $\omega_i = \omega_B$. For example, for $\omega_s = \omega_B$ and $N = 70$, the gain G^- may increase by about one order of magnitude when the pump intensity is doubled, as shown in Fig. 5(a). However, when $\omega_p = \omega_B$, this type of behavior is weaker. Also, as the number of layers N increases, the peak gain occurs at lower values of the pump intensity. Interestingly, when $\omega_s = \omega_B$ and the pump intensity $I_0^{(p^+)}$ exceeds the value at which the gain is maximum, the forward gain turns into strong attenuation since the signal wave is completely reflected, i.e. the resonance state at ω_B is changed into a forbidden state, as depicted in Fig. 5(a). Our interpertation of this result is that the signal waves generated by multiple reflections add up destructively due to an additional phase shift imparted by the

#92269 - $15.00 USD Received 30 Jan 2008; revised 18 Mar 2008; accepted 19 Mar 2008; published 1 Apr 2008

nonlinear process. This interesting transition from strong gain into strong attenuation by control of the pump intensity suggests that the device may be used as an optical switch.

In the limit of the undepleted pump approximation, neglecting material dispersion and considering small gain within each layer of the multilayered stack, the device switching behavior can be described by the following approximate expression for the forward gain

$$G^{+} \approx \left(\frac{1}{1 - I_0^{(p^+)}/I_{th}} \right)^2, \tag{28}$$

where I_{th} is a pumping threshold related to the total number of layers, the dimensions and the refractive indexes of the alternating layers of the structure as well as the nonlinear coefficients. For $I_0^{(p^+)} << I_{th}$, the gain is unity and the amplifier acts as a transparent medium. The gain increases with the pump intensity until the pumping threshold is reached. When $I_0^{(p^+)} >> I_{th}$, the gain decreases as the inverse square of $I_0^{(p^+)}$ so that the device behaves as an optical switch with a large extinction ratio.

3.3. *Optical frequency conversion*

In OFC, a signal wave u is frequency upconverted to another wave w via the pump wave v. Here; $u = s$, $v = p$, $w = i$, and $\omega_s + \omega_p = \omega_i$. The elements of the signal-idler parametric-interaction matrix of the kth layer are the same as those obtained for the OPA except,

$$\begin{aligned}
C_{k\,(s^{\pm},i^{\pm})} &= \mp j \frac{g_k^{(s)}\, \overline{a}_k^{(p^{\pm})^*}}{\gamma_k^{\pm}} \exp\left[\mp\sigma_k (l_k + 2z_{k-1})\right] \sinh\left(\gamma_k^{\pm} l_k\right), \\
C_{k\,(i^{\pm},s^{\pm})} &= \mp j \frac{g_k^{(i)}\, \overline{a}_k^{(p^{\pm})}}{\gamma_k^{\pm}} \exp\left[\pm\sigma_k (l_k + 2z_{k-1})\right] \sinh\left(\gamma_k^{\pm} l_k\right), \\
\gamma_k^{\pm} &= \left(\sigma_k^2 - g_k^{(s)} g_k^{(i)} \left| \overline{a}_k^{(p^{\pm})} \right|^2 \right)^{1/2}.
\end{aligned} \tag{29}$$

Also, the perturbed spatial dependence of the forward and backward pumps have the same form as before but with different coefficients:

$$\begin{aligned}
\alpha_k^{\pm} &= \mp j \left(\frac{g_k^{(i)}\, \overline{a}_k^{(p^{\pm})}}{\gamma_k^{\pm}} \left| a_k^{(s^{\pm})} \right|^2 - \frac{g_k^{(s)}\, \overline{a}_k^{(p^{\pm})^*}}{\gamma_k^{\pm^*}} \left| a_k^{(i^{\pm})} \right|^2 \right) \mp \rho_k^{\pm^*} a_k^{(s^{\pm})^*} a_k^{(i^{\pm})} \left(\frac{\sigma_k}{\gamma_k^{\pm}} - \frac{\sigma_k^*}{\gamma_k^{\pm^*}} \right), \\
\beta_k^{\pm} &= \mp j \left(\frac{g_k^{(i)}\, \overline{a}_k^{(p^{\pm})}}{\gamma_k^{\pm}} \left| a_k^{(s^{\pm})} \right|^2 + \frac{g_k^{(s)}\, \overline{a}_k^{(p^{\pm})^*}}{\gamma_k^{\pm^*}} \left| a_k^{(i^{\pm})} \right|^2 \right) \mp \rho_k^{\pm^*} a_k^{(s^{\pm})^*} a_k^{(i^{\pm})} \left(\frac{\sigma_k}{\gamma_k^{\pm}} + \frac{\sigma_k^*}{\gamma_k^{\pm^*}} \right), \\
\xi_k^{\pm} &= \frac{1}{\left|\gamma_k^{\pm}\right|^2} \left[\rho_k^{\pm^*} a_k^{(s^{\pm})^*} a_k^{(i^{\pm})} \left(\left|\gamma_k^{\pm}\right|^2 - |\sigma_k|^2 \right) + \rho_k^{\pm} g_k^{(s)} g_k^{(i)} a_k^{(s^{\pm})} a_k^{(i^{\pm})^*} \left| \overline{a}_k^{(p^{\pm})} \right|^2 \right. \\
&\qquad \left. - j g_k^{(i)}\, \sigma_k^* \overline{a}_k^{(p^{\pm})} \left| a_k^{(s^{\pm})} \right|^2 - j g_k^{(s)}\, \sigma_k \overline{a}_k^{(p^{\pm})^*} \left| a_k^{(i^{\pm})} \right|^2 \right], \\
\delta_k^{\pm} &= \rho_k^{\pm^*} a_k^{(s^{\pm})^*} a_k^{(i^{\pm})} - \xi_k^{\pm}.
\end{aligned} \tag{30}$$

The principal measures of the performance of the OFC device are the forward and backward conversion efficiencies,

$$\eta^{+} = \frac{I_N^{(i^+)}}{I_0^{(s^+)}}, \qquad \eta^{-} = \frac{I_0^{(i^-)}}{I_0^{(s^+)}}, \tag{31}$$

#92269 - $15.00 USD Received 30 Jan 2008; revised 18 Mar 2008; accepted 19 Mar 2008; published 1 Apr 2008

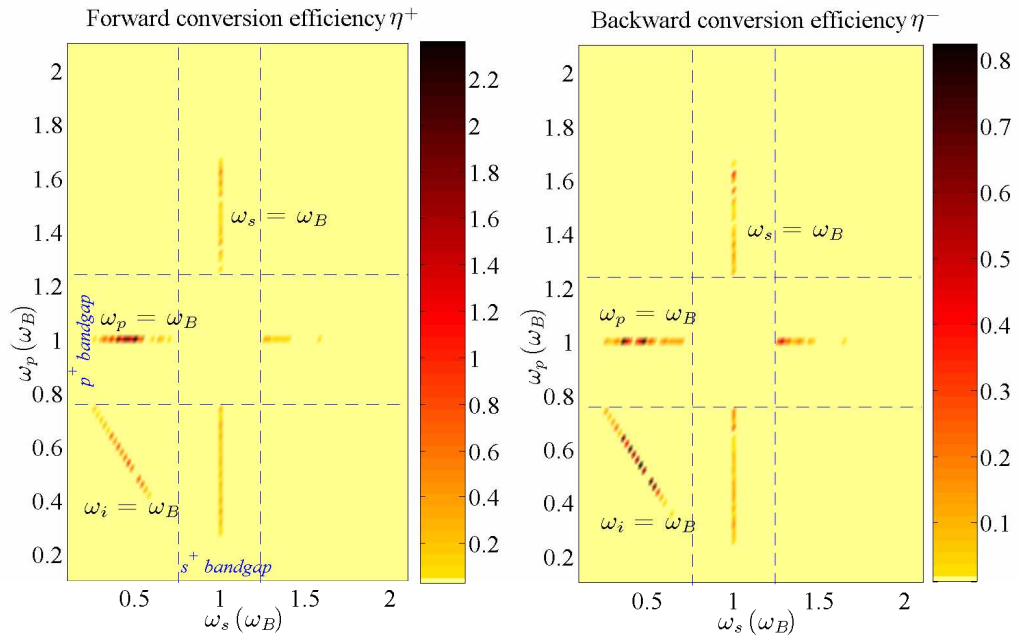

Fig. 6. (Color online). Dependence of the forward and backward conversion efficiencies on the signal and pump frequencies in units of ω_B. The dashed lines represent band-boundaries. The bright spots represent values of conversion efficiencies. The pump and signal intensities are 50 kW/cm^2 and 0.1 kW/cm^2, respectively, and the number of layers is 70. The forward and backward conversion efficiencies are enhanced at $\omega_p = \omega_B$, $\omega_s = \omega_B$ and $\omega_i = \omega_B$.

where $I_N^{(i^+)}$ and $I_0^{(i^-)}$ are the output intensities of the forward and backward upconverted wave i, respectively.

The dependence of the conversion efficiency (forward and backward) on the signal and pump frequencies is depicted in Fig. 6. The intensities of the interacting waves and the structure characteristics are the same as those described in Sec. 3.2 for the OPA. The degenerate case, $\omega_p = \omega_s$, which corresponds to SHG, is excluded from this simulation. Strong nonlinear effects emerge if one of the interacting waves is at the midgap resonance frequencies ω_B and $3\omega_B$. However, these effects are lost when $\omega_i = 3\omega_B$ because of the material dispersion that causes the disappearance of the second midgap resonance. In contrast to a bulk homogeneous medium, the total conversion efficiency, $\eta^+ + \eta^-$, can exceed unity at some frequencies without violating the conservation of energy. This is because there are two sources for the upconverted wave i: the signal wave s and the multiple reflections inside the cavity. This suggests that this device can operate simultaneously as an efficient converter and amplifier. Our iterative perturbative technique in this case reduces the maximum error Δ from 3×10^{-3} to 4×10^{-5}. We have also examined the dependence of the forward and backward conversion efficiencies on the pump intensities and found bell-shaped behavior similar to the OPA case. For $\omega_p = \omega_B$, we observed some oscillations at higher intensities (beyond the peak of the bell-shaped graph).

4. Conclusion

We have developed a generalized matrix-based model for describing second-order parametric interactions in arbitrary one-dimensional multilayered structures. The formalism accounts for

#92269 - $15.00 USD Received 30 Jan 2008; revised 18 Mar 2008; accepted 19 Mar 2008; published 1 Apr 2008

the partial depletion of the pump and is applicable to collinear oblique waves. We have used this formalism to study the performance of SHG, OPA and OFC in photonic-crystal microcavity (PCM) structures. Our results show that PCM structures have dramatically enhanced nonlinear interactions and may therefore be operated at lower levels of pump power, in comparison with conventional bulk crystals (homogeneous or quasi-phase matched) of the same overall physical length. Wave localization in PCM structures turned out to be more important for enhancing nonlinear interactions than meeting the phase matching condition. A number of interesting characteristics of PCM parametric devices have been demonstrated and proposed. For example, confirming previous reports in the literature, we found that the SHG conversion efficiency depends exponentially on the number of layers of the PCM structure. Also, because the PCM structure allows for inherently coupled forward and backward waves, devices based on OPA and OFC can be used in a bidirectional modality. In OPA, the dependence of the forward gain on the pump intensity turned out to follow a resonance-like graph with the large peak gain turning into strong attenuation at greater intensities. This large exctinction ratio suggests that the device may be used as an optical switch controlled by the pump intensity. These unique nonlinear characteristics of PCM structures are expected to enable low-power all-optical signal processing devices for microscale photonic chips.

Acknowledgements

This work was supported by a U. S. Army Research Office (ARO) Multidisciplinary University Research Initiative (MURI) Grant; and the Center for Subsurface Sensing and Imaging Systems (CenSSIS), an NSF Engineering Research Center.

#92269 - $15.00 USD Received 30 Jan 2008; revised 18 Mar 2008; accepted 19 Mar 2008; published 1 Apr 2008